Supplementary Information

Unveiling the Charge Storage Mechanism of a Supercapacitor Constructed by *Ortho*-quinone-derived Covalent Organic Framework on Electrophoretically Exfoliated Graphene

Ritika Jaryal[1†], Bharat Bhushan Upreti[2†], Parteek Kumar[1], Sanjeeb Sutradhar[1]*, Sadhika Khullar[1]*, Ramendra Sundar Dey[2]*, Rakesh Kumar[1]*

[1]Dr. B. R. Ambedkar National Institute of Technology Jalandhar, Jalandhar-144008, Punjab, India
[2]Institute of Nano Science and Technology (INST), Sector-81, Mohali-140306, Punjab, India
[†]Authors have contributed equally

Corresponding author emails: rakeshkumar@nitj.ac.in (RK), khullars@nitj.ac.in (SK), rsdey@inst.ac.in (RSD), sanjeeb.pubs@gmail.com (SS)

Table of Contents

1. General Information

1.1. Chemicals:

9,10-Phenanthrenequinone,5'-(4-formylphenyl)-[1,1':3,1"-terphenyl]-4,4"-dicarbaldehyde, potassium nitrate (KNO_3), sulphuric acid (H_2SO_4), sodium sulphide ($Na_2S{\bullet}xH_2O$), mesitylene, 1,4-dioxane, acetone, dichloromethane (DCM), tetrahydrofuran (THF), methanol, N,N-dimethylformamide (DMF) were purchased from Avra. All the chemical reagents were of analytical grade and were used without further purification.

1.2. Infrared Spectroscopy

COF was characterized by using ATR-IR BUKER ALPHA II, Germany in a range of 4000-650 cm^{-1} operating at ambient temperature.

1.3. ^{13}C Solid-State Nuclear Magnetic Resonance (NMR) Spectroscopy

Solid-state ^{13}C NMR analysis was done using ECZR Series 600 MHz NMR Spectrometer with 20 K Hz spinning speed and variable temperature range between -20 °C to +80 °C.

1.4. Powder X-ray diffraction:

Powder X-Ray diffraction patterns of the samples were recorded with Bruker D8 advance X-ray diffractometer using (Cu Kα λ=0.15406 nm) to assess the crystalline nature of the prepared material. The data analysis was performed using the Reflex module of the Materials Studio 8.0.

1.5. X-ray photoelectron spectroscopy

The chemical composition of the framework was characterized using X-ray photoelectron spectroscopy which was conducted at room temperature using a Nexsa (ThermoFisher Scientific) instrument with an Al Kα X-ray source.

1.6. Field Emission-Scanning Electron Microscopy (FE-SEM)

The morphology and size of the COF was determined using FE-SEM (CARL ZEISS GEMINI 1 SIGMA 500 VP).

1.7. High resolution Transmission Electron Microscopy (HR-TEM)

HR-TEM with charge couple device (CCD) coupled device within the working voltage range of 80 to 200 kV.

1.8. Thermo-gravimetric analysis

Thermal stability of the COF was studied by SII EXSTAR 6000 TGA thermal analyzer at a heating rate of 10 °C/min within temperature range of 30°-600 °C.

1.9. Computational method

Density functional theory (DFT) calculations were performed using Gaussian 16 set of programs.[S1] The ground state geometries of INIT-1 COF and its repeating unit of INIT-1 as well as graphene were optimized with Beck-3-parameters-Lee-Yang-Parr hybrid (B3LYP) functional together with the 3-21G basis set.[S2-S4] The 2×4 nm size of hydrogen passivated graphene sheet structure was used to consider the effect on the COF.

1.10. Electrochemical Characterizations

All cyclic voltametric (CV), Galvanostatic charge discharge (GCD), and Electrochemical impedance spectroscopic (EIS) measurements were performed in Biologic VSP-128 system electrochemical workstation. A three-electrode assembly with GCE (0.071 cm^2) working electrode, platinum wire as a counter, and Ag/AgCl (3.5 M KCl) as a reference electrode in 1 M H_2SO_4.

1.11. Electrode fabrication

The glassy carbon electrode (GCE) was chosen for the supercapacitor study. The INIT-1-EGR nanohybrid ink was drop-cast onto the surface of GCE. Before the drop-casting, the GCE surface was cleaned using the alumina powder 0.05 μm, then ultrasonicated in DI, followed by IPA. INIT-1-EGR ink was prepared by taking the quantitative amount of INIT-1-EGR nanohybrid in 1:1 (v/v) water and IPA with 5μL Nafion in 1 mL mixture. The GCE was loaded with 0.6 mg cm^{-2} of ink.

1.12. Specific Capacitance Calculations

The areal-specific capacitance C_{sp} (mF cm^{-2}) can be calculated from cyclic voltammetry (CV) from the following equation

$$C_{sp} = \frac{I(V)}{2.A.\nu.V} \qquad \text{(i)}$$

where A (in cm^2) is the geometric area, ν is the voltage scan rate (V s^{-1}), V (in V) is the potential window of the CV curves, and I(V) is current at different potentials.

Alternatively, the specific capacitance for the electrodes can be obtained from GCD data according to the following equation.

$$C_{sp} = \frac{I}{A\frac{dV}{dt}} \qquad \text{(ii)}$$

Where C_{sp} is the specific capacitance (mF cm^{-2}), I is current (A), dV/dt is the discharge slope after the IR drop, and A is the geometrical area of the single electrode.

The area normalized energy density E_A and power density P_A were calculated from galvanostatic GCD curves by the following equations

$$E_A = \frac{1}{2}.\frac{C_{sp}.\Delta V^2}{3.6} \quad \text{(iii)}$$

$$P_A = \frac{E}{\Delta t}3.6 \quad \text{(iv)}$$

where E_A is the energy density (m Wh cm^{-2}), P_A is the power density (kW cm^{-2}), C_{sp} is the specific capacitance, ΔV is the potential window ($\Delta V = V_{max} - V_{drop}$), Δt is the discharge time (s).

1.13. Dunn Method

The Dunn method is employed to measure the contributions of surface capacitive effects (electrical double layer capacitance) and diffusion-controlled effects (pseudocapacitance).[S5]The current density [$I_{(V)}$] obtained from the CV curve at a fixed potential is represented as a combination of two components.

$$I_{(V)} = k_1 v + k_2 v^{0.5} \quad \text{(v)}$$

Here, $k_1 v$ denotes the contribution from EDLC behavior, while $k_2 v$ signifies the contribution from pseudocapacitive behaviour. On dividing eq. (v) with $v^{0.5}$, the obtained equation is as follows:

$$I_{(V)}/v^{0.5} = k_1 v^{0.5} + k_2 \quad \text{(vi)}$$

A graph is plotted between $I_{(V)}/v^{0.5}$ vs. $v^{0.5}$ by obtaining $I_{(V)}$ from CVs at various scan rates. A linear trendline is fitted to calculate k_1 and k_2 which are fitted back to eq. (v) to calculate the percentage contribution from EDLC and pseudocapacitive behaviors.

2. Methods for INIT-1 and INIT-1-EGR Synthesis

2.1. Synthesis of 2,7-dinitrophenanthrene-9,10-dione

2.0 g of 9, 10-phenanthrene quinone (9.6 mmol) was dissolved in a mixture of fuming nitric acid and concentrated sulfuric acid (95-98%) under ice cold conditions. Then, the reaction mixture was allowed to stir at 100 ºC for one hour. The resulting deep orange colored solution was poured into 100 mL of ice and neutralized to pH = 7.0 using sodium hydrogen bicarbonate as a base. Yellow colored precipitates were filtered, thoroughly washed with water, dried in oven and then,

recrystallized from acetic acid to afford 1.2 g of the desired product (41.9%). ^{1}H NMR (DMSO-d_6, 500 MHz, ppm): 8.73 (s, 2H), 8.71 (s, 2H), 8.59 (s, 2H) (Figure S1).[S5]

Scheme S1: Schematic representation for the synthesis 2,7-dinitrophenanthrene-9,10-dione.

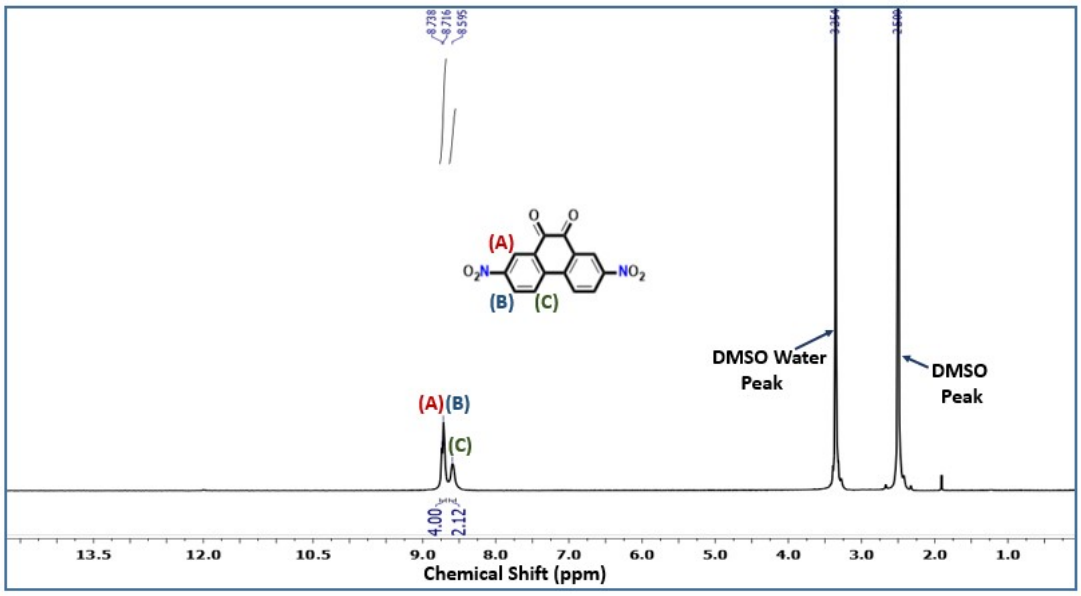

Fig. S1: ^{1}H NMR spectrum of 2,7-dinitrophenanthrene-9,10-dione (DMSO-d_6, 500 MHz).

2.2. Synthesis of 2,7-diaminophenanthrene-9,10-dione

In a 250 mL round bottom flask 2,7-dinitrophenanthrene-9,10-dione (1.0 g, 3.35 mmol) was dissolved in 50.0 mL DMF. Further, sodium sulfide ($Na_2S{\bullet}xH_2O$) (10.0 g, 37.03 mmol) was added to the reaction mixture and sonicated for 10-15 minutes and then, the mixture was stirred at 80 °C for 6 hours. The reaction mixture was diluted with water and the product was extracted slowly using ethyl acetate. Ethyl acetate layer was evaporated using rotary evaporator and further purification was done by hexane washing of the solid crude mixture using sintered funnel. Dark blue precipitates were collected and dried to afford pure product of 470.0 mg (58.8%). ^{1}H NMR (DMSO-d_6, 500 MHz, ppm): 7.64 (d, J = 11.0 Hz, 2H), 7.07 (d, J = 3.0 Hz, 2H), 6.84 (dd, J_1 = 3.3 Hz, J_2 = 11.0 Hz, 2H), 5.54 (s, 4H) (Figure S2).[S6]

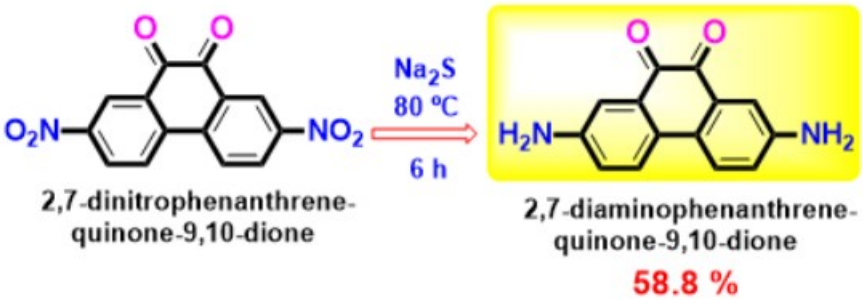

Scheme S2: Schematic representation for the synthesis of 2,7-diaminophenanthrenequinone-9,10-dione.

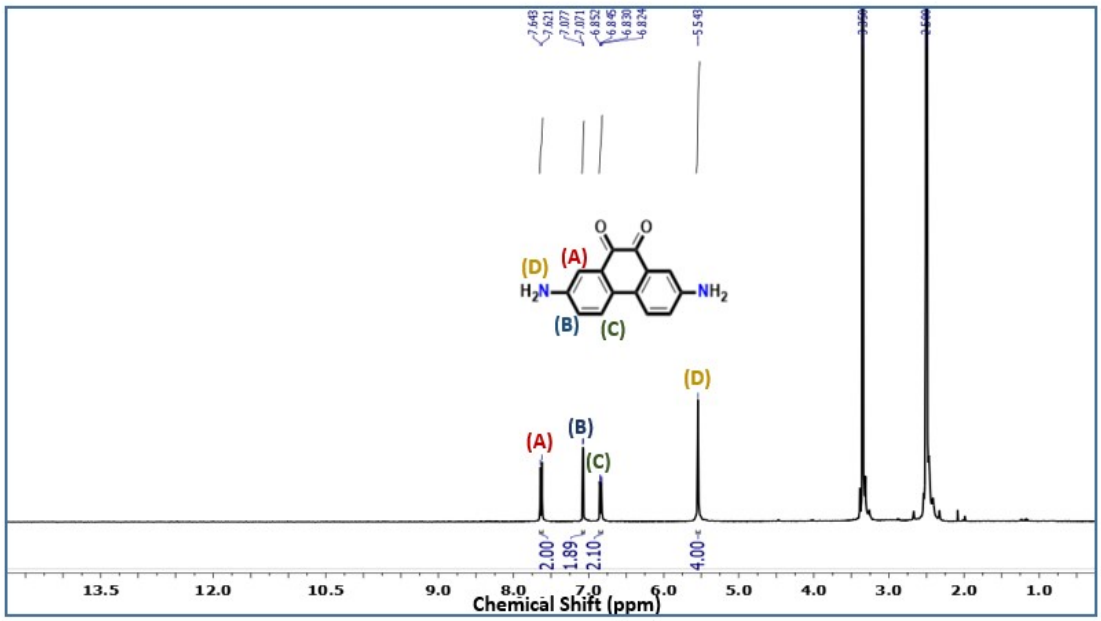

Fig. S2: ^{1}H NMR spectrum of 2,7-diaminophennthrene-9,10-dione (DMSO-d_6, 500 MHz).

2.3. Synthesis of INIT-1

An Erlenmeyer flask was charged with 2,7-diamino-9,10-phenanthrenequinone (45.0 mg, 0.19 mmol) and 5'-(4-formylphenyl)-[1,1':3,1"-terphenyl]-4,4"-dicarbaldehyde (44.0 mg, 0.11 mmol) followed by addition of 5.0 mL of (1:1) mesitylene: dioxane solvent mixture. The reaction mixture was homogenized by sonication for 10 minutes. To the obtained blue colored suspension, 6.0 M AcOH (800.0 µL) was added then, transferred to reactor. The mixture was heated for 3 days at 120 °C. Deep blue colored precipitates were filtered and washed with *N,N*-dimethyl formamide, DCM, methanol and THF, respectively and then, Soxhlet treatment was given using acetone for 18h. The obtained precipitated were dried in an oven for 24 h at 80 °C to afford 22.0 mg of black powder.

2.4. Synthesis of INIT-1-EGRX

The synthesis of INIT-1-EGRX nanohybrid was done via a quick *in-situ* exfoliation method in an electrochemical setup with 2 graphite electrodes. A constant potential of 3.5 V was applied on the graphite plate (1x3 cm^2) dipped in 1.5 M H_2SO_4 solution for a time limit of 10 min, 15 min, and 20 min, respectively, for INIT-1-EGR10, INIT-1-EGR15 (INIT-1-EGR), and INIT-1-EGR20. The electrophoretic exfoliation formed a black mass in the solution, and agglomeration was removed by sonicating the solution for 30 min. The dispersed solution was then pH neutralized with centrifugation with DI water, the supernatant was discarded, and the residue was kept overnight in a hot air oven at 50 °C.

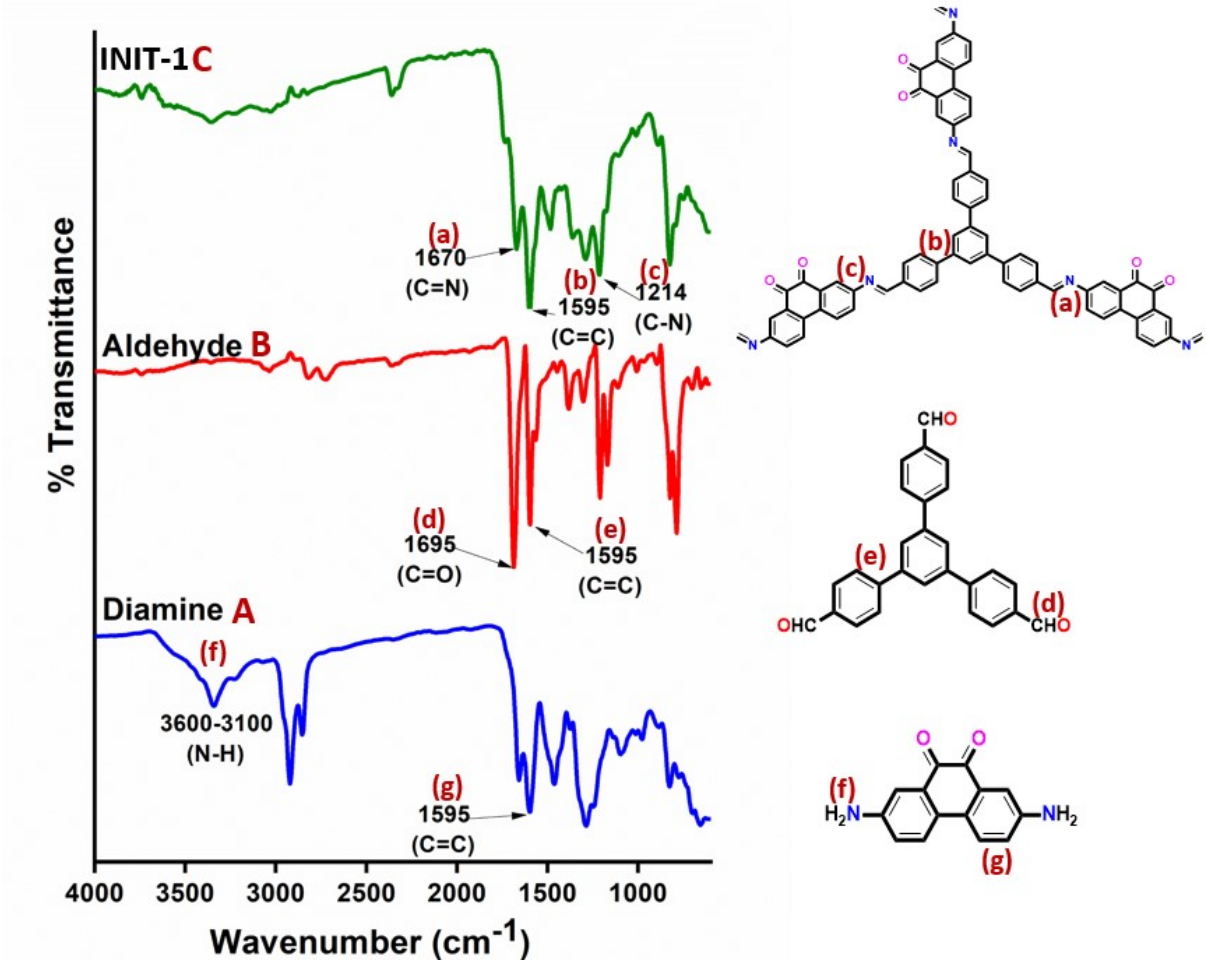

Fig. S3: ATR-IR spectra of 2,7-diaminophenanthrene-9,10-dione (A); 5'-(4-formylphenyl)-[1,1':3,1"- terphenyl]-4,4"-dicarbaldehyde (B); and INIT-1 COF (C).

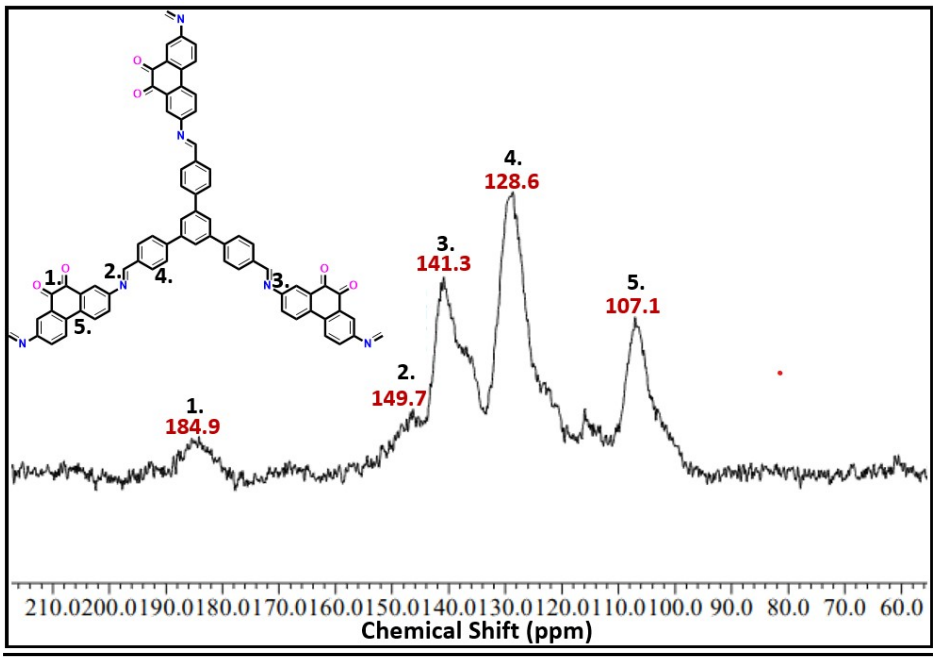

Fig. S4: ^{13}C CP-MAS solid-state NMR spectrum of COF INIT-1.

Table S1: Atomic coordinates for the repeating unit of INIT-1 COF

Space group: P6/m, Hexagonal. **Lattice Parameters**: a = 34.99 Å; b = 34.99 Å; c = 3.49 Å; $\alpha = \beta = 90°$, $\gamma = 120°$

Atom	x	y	z
C1	32.38	-25.96	0
C2	32.38	-27.4	0
C3	33.62	-28.12	0
C4	34.87	-27.4	0
C5	34.87	-25.96	0
C6	33.62	-25.24	0
C7	33.62	-23.8	0
C8	31.13	-28.11	0
C9	36.11	-28.11	0
C10	36.11	-29.55	0
C11	37.36	-30.27	0
C12	38.61	-29.55	0
C13	38.61	-28.11	0
C14	37.36	-27.39	0
C15	29.89	-27.39	0

C16	**28.64**	**-28.11**	**0**
C17	**28.64**	**-29.55**	**0**
C18	**29.89**	**-30.27**	**0**
C19	**31.13**	**-29.55**	**0**
C20	**34.87**	**-23.08**	**0**
C21	**34.87**	**-21.64**	**0**
C22	**33.62**	**-20.92**	**0**
C23	**32.38**	**-21.64**	**0**
C24	**32.38**	**-20.92**	**0**
C25	**39.85**	**-30.27**	**0**
C26	**27.4**	**-30.27**	**0**
C27	**33.62**	**-19.49**	**0**
N28	**26.15**	**-29.55**	**0**
N29	**41.09**	**-29.55**	**0**
N30	**32.38**	**-18.77**	**0**
C31	**42.34**	**-30.27**	**0**
C32	**24.91**	**-30.27**	**0**
C33	**32.38**	**-17.33**	**0**
C34	**42.34**	**-31.71**	**0**
C35	**43.58**	**-32.43**	**0**
C36	**44.83**	**-31.71**	**0**
C37	**44.83**	**-30.27**	**0**
C38	**43.58**	**-29.55**	**0**
C39	**46.08**	**-32.43**	**0**
C40	**47.32**	**-31.71**	**0**
C41	**47.32**	**-30.27**	**0**
C42	**46.08**	**-29.55**	**0**
C43	**46.08**	**-33.87**	**0**
C44	**47.32**	**-34.59**	**0**
C45	**48.57**	**-33.87**	**0**
C46	**48.57**	**-33.87**	**0**
N47	**49.81**	**-32.43**	**0**

C48	**51.06**	**-33.87**	**0**
O49	**46.08**	**-28.12**	**0**
O50	**48.57**	**-29.55**	**0**

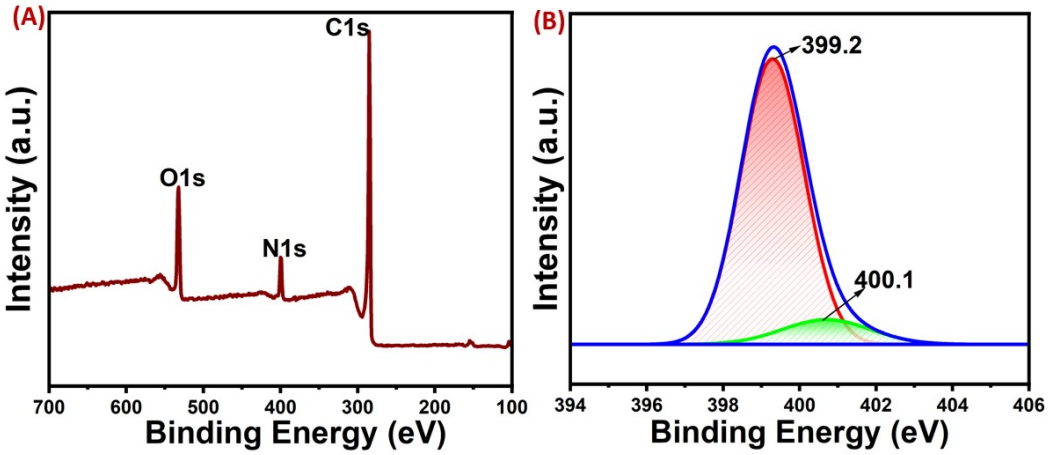

Fig. S5: XPS spectra of INIT-1 (A); and deconvoluted N1s XPS spectra of INIT-1 COF(B).

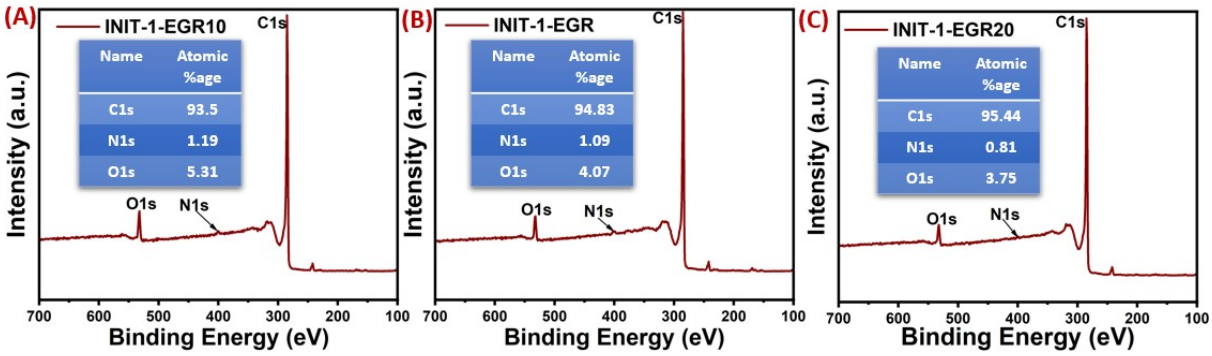

Fig. S6: XPS spectra of INIT-1-EGR10 (A); INIT-1-EGR (B) and INIT-1-EGR20 with their atomic percentages.

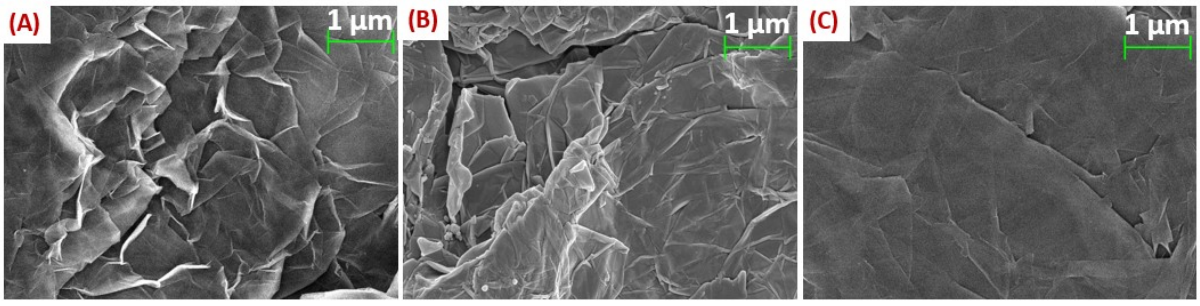

Fig. S7: FE-SEM images of INIT-1-EGR10 (A); INIT-1-EGR (B) and INIT-1-EGR20.

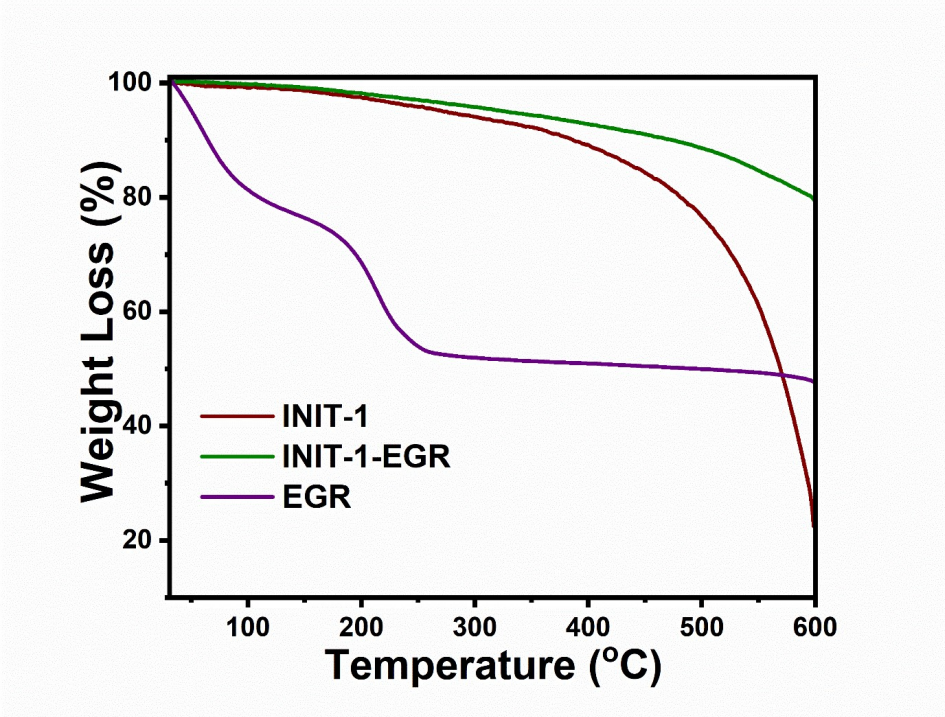

Fig. S8: TGA scans of INIT-1; INIT-1-EGR and EGR.

Table S2: DFT calculated (using 3-21G basis set) ground state energy for INIT-1 COF, its repeating unit, and hydrogen passivated graphene

Molecules	**Ground state energy (kcal/mol)**
INIT-1 COF	-7084.58×10^3
Repeating unit of INIT-1 COF	-1727.19×10^3
Hydrogen passivated graphene	-8106.99×10^3

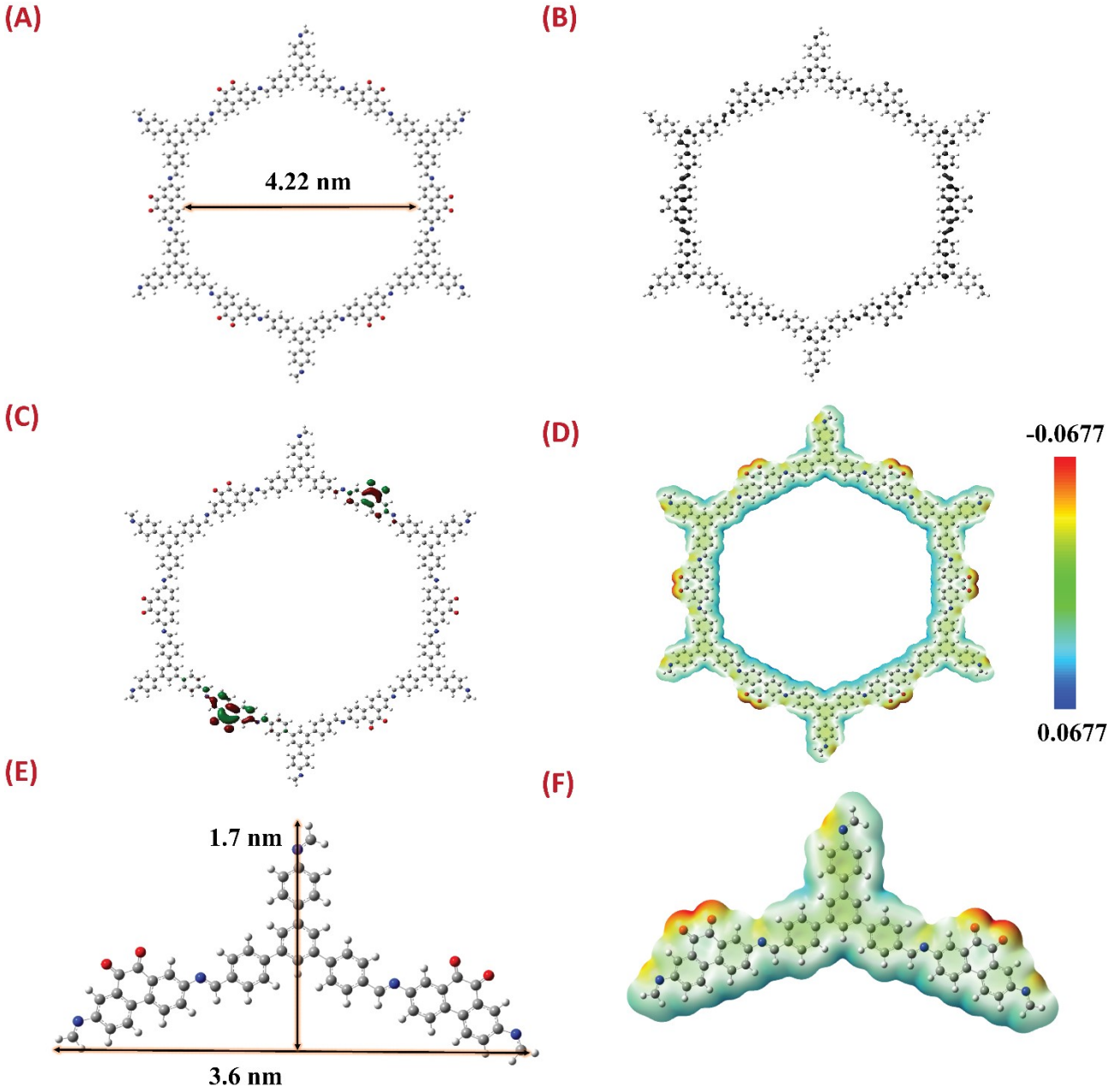

Fig. S9: DFT-B3LYP/3-21G optimized geometry (A); HOMO (B); LUMO (C); and ESP (D) map of INIT-1 COF. DFT-B3LYP/3-21G optimized geometry (E); and the corresponding ESP (F) map of the repeating unit of INIT-1 COF.

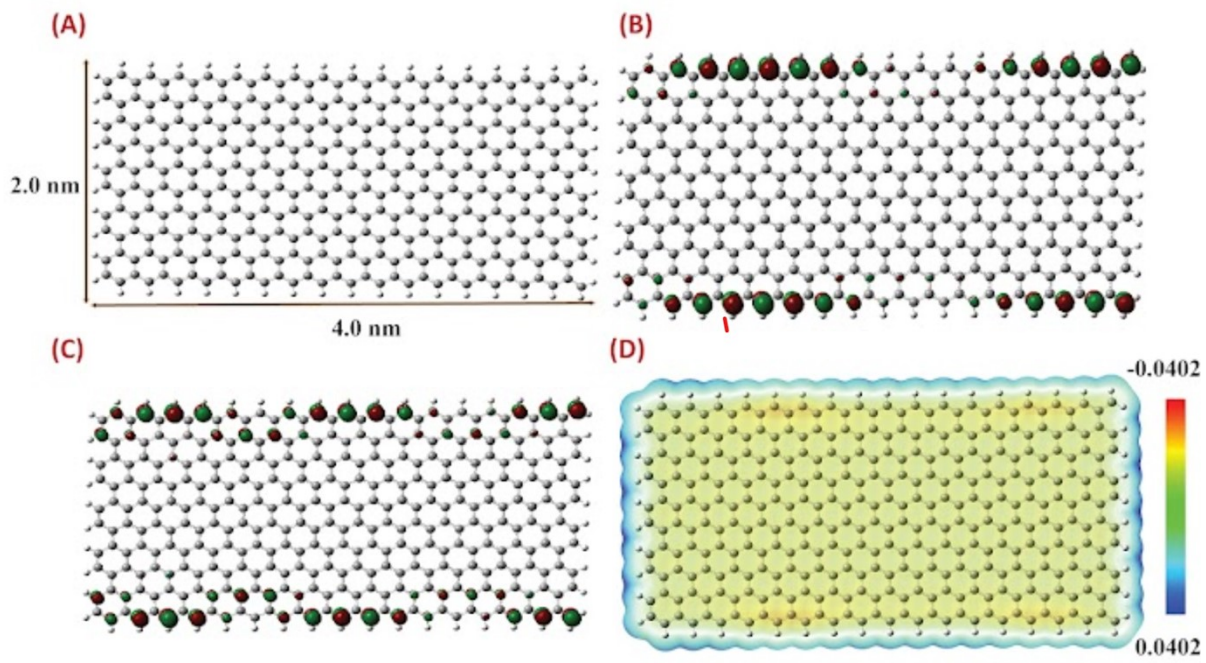

Fig. S10: DFT-B3LYP/3-21G optimized geometry (A); HOMO (B); LUMO (C); and ESP (D) map of hydrogen passivated graphene (size 20 × 40 Å).

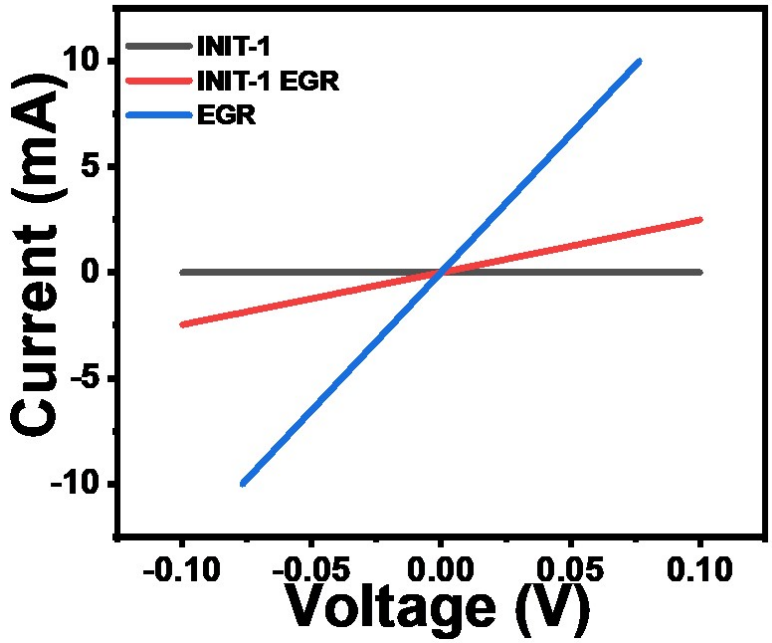

Fig. S11: I-V characteristic curve for INIT-1 COF, EGR and INIT-1 EGR nanohybrid.

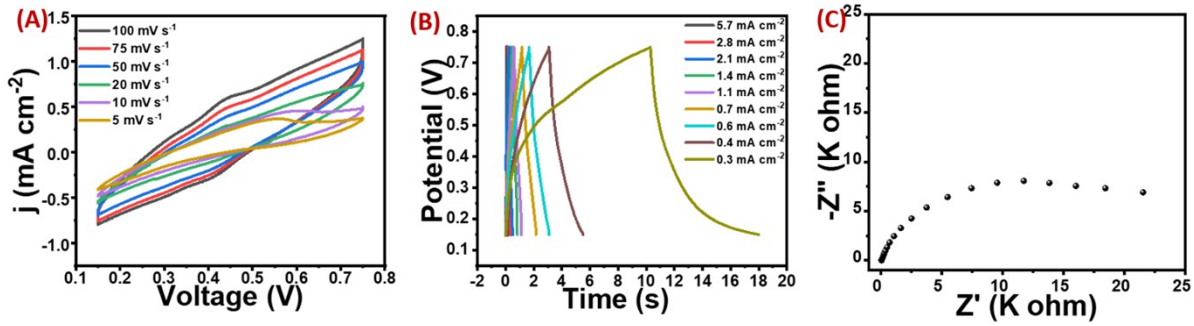

Fig. S12: CV(A); GCD (B); and EIS plot (C)of INIT-1, showing a capacitance value of 7.5 mF cm^{-2} @ 5 mV s^{-1}.

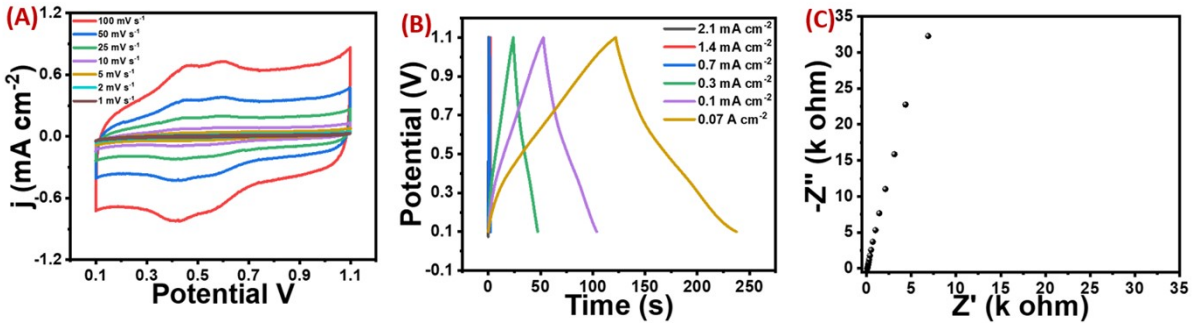

Fig. S13: CV (A); GCD (B); and EIS plot (C) of INIT-1-EGR10, showing a capacitance value of 6.21 mF cm^{-2} @ 1mV s^{-1}.

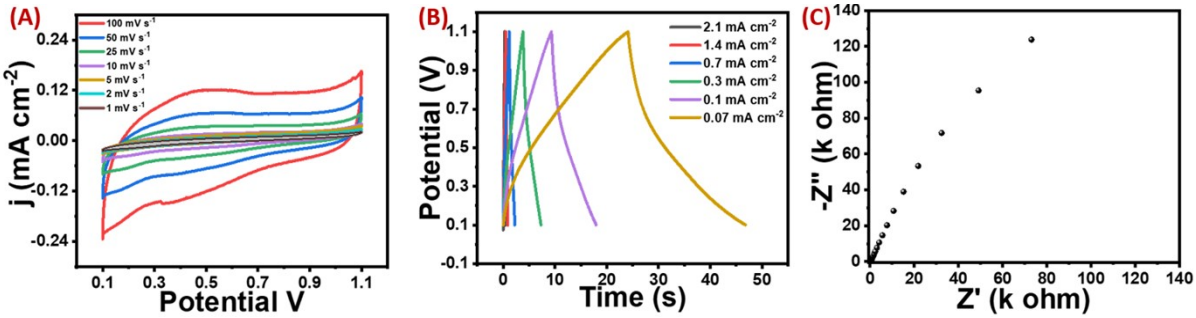

Fig. S14: CV (A); GCD (B); and EIS plot (C) of INIT-1-EGR20, showing a capacitance value of 3.45 mF cm^{-2} @ 1mV s^{-1}.

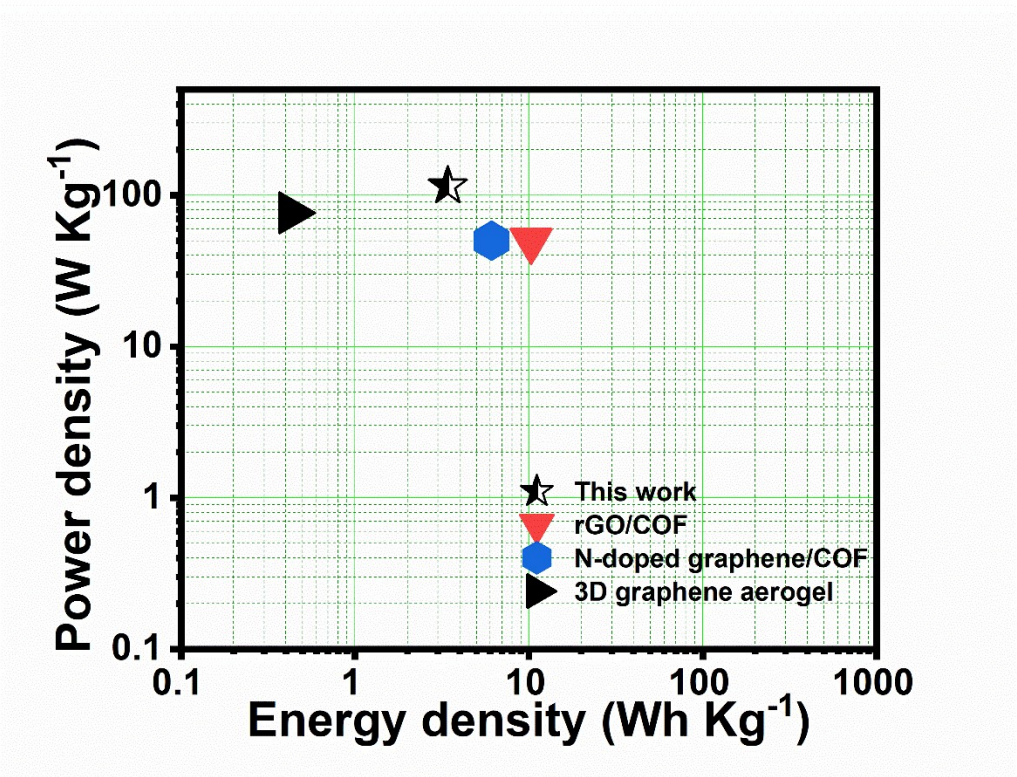

Fig. S15: Ragone Plot of INIT-1 EGR with comparable work including rGO/COF, N-doped graphene/COF and 3D graphene aerogel.

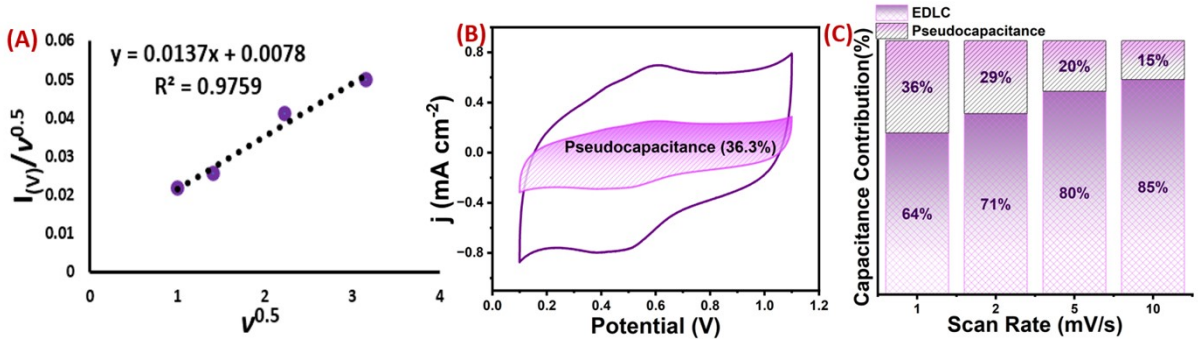

Fig. S16: Linear fitting curve of current densities with various scan rates (1 mV s^{-1} to 10 mV s^{-1}) at a fixed potential of 0.6 V (A); calculation of capacitance contribution at a scan rate of 1.0 mV s^{-1}. The purple region outlined the capacitance contributed from pseudocapacitance (B); capacitance contribution (%) evaluated at various scan rates (C).

Table S3: Comparison of the capacitive performance of materials reported in this work with other reported supercapacitive materials

Name	Electrolyte	Areal Capacitance	Retention Cycles	Ref.
INIT-1-EGR	1.0 M H_2SO_4	15.42 mF cm^{-2}	112% (5500)	This Work
INIT-1 COF	1.0 M H_2SO_4	7.5 mF cm^{-2}	-	
INIT-1-EGR10	1.0 M H_2SO_4	6.21 mF cm^{-2}	-	
INIT-1-EGR20	1.0 M H_2SO_4	3.45 mF cm^{-2}	-	
COF-316@PPy	2.0 M H_2SO_4	783.6 µF cm^{-2}	100% (3400)	S8
Graphene	30 wt% KOH	64 µF cm^{-2}	~90% (1200)	S9

CTDq1Da1Tp	1.0 M H_2SO_4	8.5 mF cm^{-2}	78% (7000)	S10
CT-DqTp	1.0 M H_2SO_4	12 mF cm^{-2}	80% (2500)	
e-JUC-511	1.0 M NBu_4PF_4/ACN	5.46 mF cm^{-2}	100% (10000)	S11
e-JUC-512	1.0 M NBu_4PF_4/ACN	5.85 mF cm^{-2}	100% (10000)	
g-$C_{34}N_6$-COF/SWCNTs	LiCl/PVA gel	15.2 mF cm^{-2}	93.1% (5000)	S12
MOF-Uio-66-NH2	$(C_2H_5)_4NBF_4$/ACN	7.89 mF cm^{-2}	69.5% (2000)	S13
MOF@COF-LZU1	$(C_2H_5)_4NBF_4$/ACN	9.65 mF cm^{-2}	73.9%% (2000)	
aza-MOF@COF	$(C_2H_5)_4NBF_4$/ACN	20.35 mF cm^{-2}	89.3% (2000)	
HKUST-1	$(C_2H_5)_4NBF_4$/ACN	2.334 mF cm^{-2}	80% (6000)	S14
ZIF-8	$(C_2H_5)_4NBF_4$/ACN	0.268 mF cm^{-2}	80% (2500)	
nMOF-867	$(C_2H_5)_4NBF_4$/ACN	5.09 mF cm^{-2}	80% (>10000)	
$COF_{DAAQ-BTA}$-graphene composite	1.0 M KOH	31.5 mF cm^{-2}	70% (500)	S15
Azulene-bridged coordination polymer framework (PiCBA)	H_2SO_4/PVA	0.1 mF cm^{-2}	86% (350)	S16
COF-MSC	LiCl/PVA	15.2 mF cm^{-2}	93.1% (5000)	S17

References:

S1. M. J. Frisch, *et al.* Gaussian 16, Revision C.01, Gaussian. Inc.: Wallingford CT, 2019.

S2. K. Liu, P. Yan, J. Li, C. He, T. Ouyang, C. Zhang, C. Tang, and J. Zhong, *Sci. Rep.,* 2017, **7**, 8461.

S3. S. Baachaoui, S. Aldulaijan, L. Sementa, A. Fortunelli, A. Dhouib, and N. Raouafi, *J. Phys. Chem. C,* 2021, **125**, 26418−26428.

S4. D. Baniya, *Kathford Eng. Manag J.,* 2018, **1**.

S5. M. Li, J. Liu, Y. Li, G. Xing, X. Yu, C. Peng and L. Chen, *CCS Chemistry*, 2020, **3**, 696-706.

S6. C. X. Liu, D. L. Pan, Y. Seo, S. Park, J. L. Kan, J. Y. Koo, W. Choi, and E. Lee, *ACS Appl. Energy Mater.,* 2023, **6**, 1126–1133.

S7. S. Zheng, D. Shi, D. Yan, Q. Wang, T. Sun, T. Ma, L. Li, D. He, Z. Tao, and J. Chen, *Angew. Chem., Int. Ed.,* 2022, **64**, e202117511.

S8. W. Wang, W. Zhao, T. Chen, Y. Bai, H. Xu, M. Jiang, S. Liu, W. Huang, Q. Zhao, *Adv. Funct. Mater.*, 2021, **31**, 2010306.

S9. Y. Wang, Z. Shi, Y. Huang, Y. Ma, C. Wang, M. Chen and Y. Chen, *J. Phys. Chem. C,* 2009, **113**, 13103–13107.

S10. A. Khayum M, V. Vijayakumar, S. Karak, M. Bhadra, K. Suresh, N. Acharambath, S. Kurungot and R. Banerjee, *ACS Appl. Mater. Interfaces*, 2018, **10**, 28139-28146.

S11. Y. Yusran, H. Li, X. Guan, D. Li, L. Tang, M. Xue, Z. Zhuang, Y. Yan, V. Valtchev, S. Qiu and Q. Fang, Adv. Mater. 2020, **32**, 1907289.

S12. J. Xu, Y. He, S. Bi, M. Wang, P. Yang, D. Wu, J. Wang and F. Zhang, *Angew. Chem., Int. Ed.*, 2019, **58**, 12065–12069.

S13. H. Peng, J. Raya, F. Richard, W. Baaziz, O. Ersen, A. Ciesielski, P. Samorì, Angew. Chem. Int. Ed., 2020, **59**, 19602-19609.

S14. K. M. Choi, H. M. Jeong, J. H. Park, Y.-B. Zhang, J. K. Kang and O. M Yaghi, ACS Nano 2014, **8**, 7451-7457.

S15. Z. Zha, L. Xu, Z. Wang, X. Li, Q. Pan, P. Hu, and S. Lei, *ACS Appl. Mater. Interfaces,* 2015, **7**, 17837−17843.

S16. C. Yang, K. S. Schellhammer, F. Ortmann, S. Sun, R. Dong, M. Karakus, Z. Mics, M. Löffler, F. Zhang, X. Zhuang, E. Cánovas, G. Cuniberti, M. Bonn and X. Feng, *Angew. Chem. Int. Ed.*, 2017, **56**, 3920-3924.

S17. J. Xu, Y. He, S. Bi, M. Wang, P. Yang, D. Wu, J. Wang and F. Zhang, *Angew. Chem. Int. Ed.,* 2019, **58**, 12065-12069.